JACS
JOURNAL OF THE AMERICAN CHEMICAL SOCIETY
pubs.acs.org/JACS
Article

Evidence for the Chemical Mechanism of RibB (3,4-Dihydroxy-2-butanone 4-phosphate Synthase) of Riboflavin Biosynthesis

Nikola Kenjić, Kathleen M. Meneely, Daniel J. Wherritt, Melissa C. Denler, Timothy A. Jackson, Graham R. Moran, and Audrey L. Lamb*

Cite This: J. Am. Chem. Soc. 2022, 144, 12769–12780
Read Online
ACCESS | Metrics & More | Article Recommendations | Supporting Information

ABSTRACT: RibB (3,4-dihydroxy-2-butanone 4-phosphate synthase) is a magnesium-dependent enzyme that excises the C4 of D-ribulose-5-phosphate (D-Ru5P) as formate. RibB generates the four-carbon substrate for lumazine synthase that is incorporated into the xylene moiety of lumazine and ultimately the riboflavin isoalloxazine. The reaction was first identified by Bacher and co-workers in the 1990s, and their chemical mechanism hypothesis became canonical despite minimal direct evidence. X-ray crystal structures of RibB typically show two metal ions when solved in the presence of non-native metals and/or liganding non-substrate analogues, and the consensus hypothetical mechanism has incorporated this cofactor set. We have used a variety of biochemical approaches to further characterize the chemistry catalyzed by RibB from *Vibrio cholera* (VcRibB). We show that full activity is achieved at metal ion concentrations equal to the enzyme concentration. This was confirmed by electron paramagnetic resonance of the enzyme reconstituted with manganese and crystal structures liganded with Mn^{2+} and a variety of sugar phosphates. Two transient species prior to the formation of products were identified using acid quench of single turnover reactions in combination with NMR for singly and fully ^{13}C-labeled D-Ru5P. These data indicate that dehydration of C1 forms the first transient species, which undergoes rearrangement by a 1,2 migration, fusing C5 to C3 and generating a hydrated C4 that is poised for elimination as formate. Structures determined from time-dependent Mn^{2+} soaks of VcRibB-D-Ru5P crystals show accumulation in crystallo of the same intermediates. Collectively, these data reveal for the first time crucial transient chemical states in the mechanism of RibB.

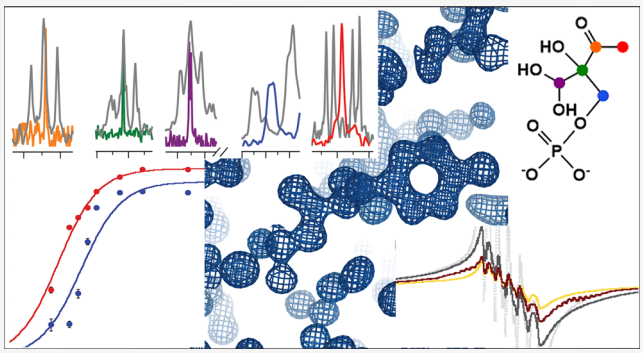

INTRODUCTION

Riboflavin is the direct precursor for the production of flavin adenine mononucleotide and subsequently flavin adenine dinucleotide, essential cofactors in redox and non-redox reactions in all forms of life.[1,2] Riboflavin is required for fundamental cellular processes, such as primary metabolism, the electron transport chain of cellular respiration, folate synthesis,[1] iron absorption,[3] DNA repair,[4] and inflammation/immune responses.[5,6] Plants, bacteria, and fungi have genes for the enzymatic production of riboflavin, but animals must obtain riboflavin (vitamin B2) from their diet. Not surprisingly, riboflavin biosynthesis has drawn attention as a target for antibacterial/antimicrobial drug design.[7−9]

Riboflavin biosynthesis has a convergent pathway with the initial substrates of the individual branches being guanosine triphosphate and D-ribulose 5-phosphate (D-Ru5P, a five-carbon sugar phosphate of the pentose phosphate pathway), both prevalent metabolites. 3,4-Dihydroxy-2-butanone 4-phosphate (DHBP) synthase, or RibB, is a magnesium-dependent enzyme that dehydrates the first carbon and removes the fourth carbon of D-Ru5P to make the four-carbon, DHBP product (Figure 1A). Evidence for this unexpected chemistry is from classic biochemistry feeding studies and endpoint assays with ^{13}C-labeled ribose, acetate, glucose, glycerol, and ribulose-5-phosphate employing ^{13}C NMR detection.[10−16] The enzyme mechanism that has been proposed is necessarily complicated and requires at least four steps: (1) dehydration at C1 to generate the methyl, (2) a skeletal rearrangement to link C3 and C5, and a (3) hydration at C4 to facilitate (4) deformylation. The order of events as accepted in the literature is shown in Figure 1B,[16] which we refer to as the "canonical" mechanism. The inversion of the stereochemistry at C3 has previously been established by CD spectroscopy (Figure 1A).[15] Due to the complexity of the reaction, it is not surprising that the RibB reaction is

Received: March 29, 2022
Published: July 8, 2022

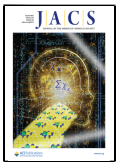

https://doi.org/10.1021/jacs.2c03376
J. Am. Chem. Soc. 2022, 144, 12769−12780

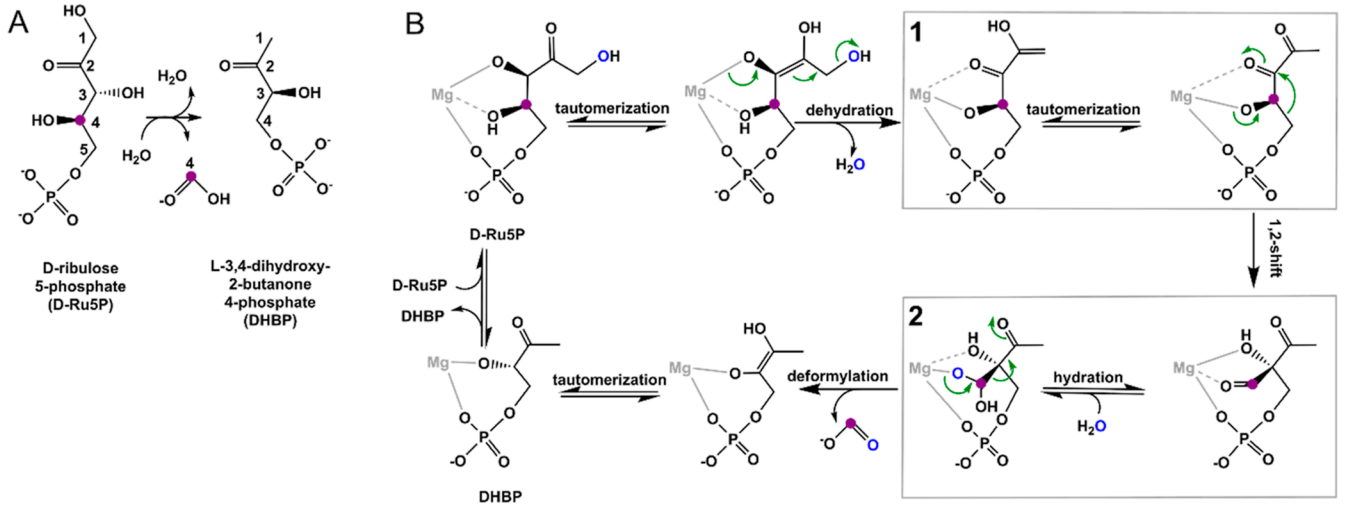

Figure 1. Hypothetical canonical mechanism depicted in the context of the findings of this study. (A) RibB catalyzes the conversion of D-ribulose 5-phosphate (D-Ru5P) to L-3,4-dihydroxy-2-butanone 4-phosphate (DHBP), dehydrating C1 and removing C4 as formate. (B) Mechanism proposed in the literature has four key steps: dehydration, 1,2-shift, hydration, and deformylation. Boxes indicate intermediate states identified in this study. Structures drawn in the Natta projection.

considered to be one of the rate-limiting steps in riboflavin biosynthesis,[17] with RibB enzymes demonstrating turnover numbers on the order of six per minute.[18]

The structure of RibB appears to be a standard $\alpha+\beta$ structure, in which α-helices pack against both sides of a central β-sheet (Figure 2). However, the connectivity of the

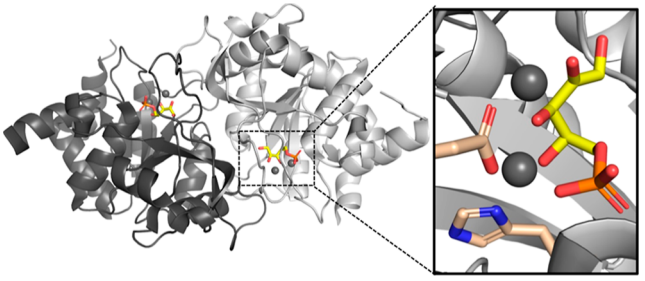

Figure 2. *V. cholerae* RibB structure (PDB: 4P8E). RibB is a dimer (monomers light and dark gray). This structure contains the D-Ru5P substrate (yellow sticks with red oxygens and orange phosphorous) and is inactivate because the required magnesium ion(s) have been substituted by the two zinc ions (gray spheres). The inset shows magnification of the active site, highlighting two residues, Glu39 and His154 colored wheat, which coordinate to the two reported metal ions and will be shown in all subsequent images of the active site.

secondary structure is unique and dictates that RibB has a distinctive fold.[19−21] Indeed, if one performs a homology search using PDBeFold[22] and sets low thresholds, 51 RibB chains are returned with very high secondary structure matching (over 80%) and strikingly similar root mean squared deviation (rmsd) (1.5 Å or less for at least 180 of 216 Cα carbons). Additionally, four protein structures of unknown function are identified, which show a clear deviation in comparison statistics (rmsd doubles, Q score halves). The active site is surrounded by two mobile loops. The shorter loop, loop 1, is composed of acidic residues that are important for binding of the substrate and metal. The longer loop, loop 2, shows conformational flexibility with the substrate and metal binding.[20,21,23]

The majority of structures reported in the PDB are for non-active states, with Mn^{2+}, Zn^{2+}, and Ca^{2+} substituted for the catalytic Mg^{2+}. Others have sulfate or phosphate in the active site, and a few have a metal and/or substrate or substrate analogues bound.[19−21,23−28] It is widely accepted that the enzyme requires two magnesium ions to be catalytically active, but this is based on noncatalytic zinc-substituted structures of a ternary protein−metal−substrate complex.[23,27] However, RibB·ribulose 5-phosphate complex structures show that the substrate binds in the absence of metal with the phosphate highly coordinated by amino acid side chains.[28] Indeed, there are several structures in which sulfate or phosphate bind in the substrate-phosphate site in the absence of metal, indicating that the metal ion is not required for substrate binding.[20,27]

We have sought to provide evidence for the chemical mechanism of RibB. Initially, we determined that RibB uses a mononuclear magnesium center for catalysis using perturbation of tyrosine fluorescence, activity assays, and electron paramagnetic resonance (EPR) data. Furthermore, we showed that RibB activity is pH dependent, which correlates with magnesium binding. Using acid quench of a single turnover reaction in combination with nuclear magnetic resonance and X-ray crystallography employing crystals grown with the native substrate and subjected to time-dependent soaks with metal ion, we identified two catalytic intermediates that accumulate in the catalytic cycle of RibB that give credence to the hypothesis of a 1,2-shift followed by deformylation for the excision of the 4-carbon from the 5-carbon D-ribulose 5-phosphate.

METHODS

RibB Overexpression and Purification. The overexpression construct for the RibB gene was prepared by GenScript. The ribB gene from *Vibrio cholerae* (*V. cholerae*) (sequence ID: AE003853.1, strain: N16961, taxid: 243277) was initially synthesized and cloned into the pUC15 vector. This gene was then transferred to the pET28a + vector that yields the VcRibB protein with an N-terminal 6 His tag. The VcRibB construct was transformed into BL21(DE3) *Escherichia coli* (*E. coli*) (New England Biolabs) and grown overnight at 37 °C in 50 mL of LB broth, Miller (Fisher) with 50 μg/mL kanamycin in a shaker incubator (250 rpm). 1L of the Miller formulation of LB broth

https://doi.org/10.1021/jacs.2c03376
J. Am. Chem. Soc. 2022, 144, 12769−12780

with 50 μg/mL kanamycin was inoculated with 10 mL of the overnight culture and grown at 37 °C in a baffled flask in a shaker incubator (250 rpm). When the culture OD_{600nm} reached 0.8, protein expression was induced with a final concentration of 0.5 mM isopropyl β-D-1-thiogalactopyranoside (IPTG) and was further incubated at 37 °C for 4 h with shaking. The cells were harvested by centrifugation (6000*g*, 10 min, 4 °C). The cell pellet was resuspended in 10 mL of 50 mM Tris-HCl (pH 8.0), 50 mM imidazole, and 500 mM NaCl per liter of culture broth. Resuspended cells were lysed by passage through a French Press three times at 13,000 psi. The cell lysate was centrifuged at 12,000*g* for 40 min at 4 °C. The supernatant was injected onto a 25 mL Chelating Sepharose Fast Flow (GE Healthcare) column charged with nickel chloride and pre-equilibrated with 50 mM Tris-HCl (pH 8.0), 50 mM imidazole, and 500 mM NaCl. The protein was eluted with a 250 mL linear gradient increasing the imidazole concentration to 500 mM imidazole (RibB eluted at ~200 mM imidazole) or with a step gradient of 300 mM imidazole. The protein was concentrated to 30 mL using an Amicon nitrogen gas-pressurized concentrator with a 10 kDa cutoff filter and injected onto a 120 mL Superdex 200 gel-filtration column (GE Healthcare), pre-equilibrated with 25 mM Tris-HCl (pH 8.0). RibB eluted as a dimer and was concentrated using an Amicon Ultracell 30 K centrifugal concentrator to 40 mg/mL, as determined by Bradford, and stored at −80 °C for later use. The purification yield was 250 mg of protein per liter of culture.

RibB Purification in the Presence of EDTA. To remove the residual divalent metal ions, prior to the size exclusion step, the protein was incubated with a final concentration of 2 mM EDTA for 10 min on ice. The buffer for the size exclusion column contained 100 μM EDTA. Before binding and activity assay experiments commenced, the protein was exchanged again into freshly made 25 mM Tris-HCl (pH 8.0), 100 μM EDTA, and concentrated to 37.7 mg/mL using an Amicon Ultracell 30 K centrifugal concentrator.

Steady-State Kinetics Varying the D-Ribulose 5-Phosphate Concentration. We adapted the previously developed assay[18,23] to compare the kinetic parameters of our purified enzyme for differing metals and sugar phosphates. A major change to the assay included using the actual sugar phosphates as substrates as opposed to the addition of pentose phosphate isomerase to generate D-ribulose 5-phosphate during assay incubation. D-ribulose 5-phosphate (D-Ru5P), D-ribose 5-phosphate (D-R5P), D-xylulose 5-phosphate (D-Xy5P), and L-xylulose 5-phosphate (L-Xy5P) (Sigma-Aldrich) were dissolved in 50 mM Tris-HCl (pH 7.5) to a concentration of 90 mM. Sugar phosphate, 10 μM enzyme, and 10 mM $MgCl_2$ were mixed to a final volume of 200 μL and incubated for 30 min at room temperature with sugar phosphate concentrations varied from 0 to 4 mM for D-Ru5P, 0−200 mM for D-R5P, 0−8 mM for D-Xy5P, and 0−20 mM for L-Xy5P. The reaction was quenched by the addition of 175 μL of freshly made 200 mM naphthol (dissolved in 1 N NaOH) and 250 μL of 270 mM creatine (dissolved in water), and the color was allowed to develop for 30 min.[18] The product was detected by an absorption scan from 450 to 650 nm using a Cary 50 Bio UV−visible spectrophotometer. The absorbance at λ_{max} (525 nm) was corrected by subtracting the absorbance at 650 nm and then converted to the concentration (in nM) using a 3,4-butadione standard curve, not the 3,4-dihydroxy-2-butanone phosphate (DHBP), as was carried out previously.[18] Values for V_{max} and K_M are averages of three trials collected twice on separate days, and errors are reported as the standard deviation of these values. The data for the biological substrate (D-Ru-5P) and metals (Mg^{2+} and Mn^{2+}) were fit to the Michaelis−Menten equation using Kaleidgraph (Synergy Software). The data for the other sugar phosphates were fit to the substrate inhibition model to give a trend line illustrative of the data, but numbers are not reported due to poor fit (see the Results section). Error propagation was used in the determination of error values for k_{cat} and k_{cat}/K_M. For the pH titration, D-Ru5P was the varied substrate, and a 100 mM succinic acid, phosphate, glycine (SPG) buffer system was used at pH values of 5.0, 5.4, 5.8, 6, 6.5, 7.0, 8.0, and 9.0, as described by Newman.[29] pH profiles of k_{cat} and k_{cat}/K_M values for substrates were fit to the following equation:

$$\log Y = \log\left[\frac{c}{1 + \frac{H}{K_a}}\right]$$

Kinetic parameters at each pH were determined in triplicate. The values presented are the averages of these three trials, and the reported errors are the standard deviation.

Steady-State Kinetics Varying the Metal Ion Concentration. The dependence of the steady-state kinetic parameters on the magnesium concentration was determined with D-Ru5P with one alteration in the procedure. The standard reaction mixture (200 μL) contained diluted $MgCl_2$ (Fisher 99.9% pure; 0−800 μM), 1.8 mM Ru5P, and 10 μM enzyme. The dependence of the steady-state kinetic parameters on the manganese concentration was obtained in the same manner as with Mg^{2+} but used 1 μM enzyme and pure $MnCl_2$ (Fisher 99% pure; 0−250 μM), and the incubation time prior to quenching was increased to 150 min.

Metal-Binding Stoichiometry. VcRibB has no tryptophan residues, and changes in intrinsic tyrosine fluorescence were used to observed metal binding. The data were measured using a Cary 50 Eclipse fluorometer with an excitation wavelength of 280 nm and emission recorded from 290 to 400 nm (excitation slit: 10 nm; emission slit: 5 nm). The 200 μL of the reaction mixture containing 50 mM tris-HCl (pH 7.5), 100 μM EDTA, 1.8 mM D-Ru5P, and 60 μM RibB [50 mM Tris-HCl, 100 μM EDTA (pH 8)] was titrated with 1 μL increments of 2 mM $MgCl_2$ and 100 μM EDTA solution. The reported Mg^{2+} concentration accounts for the dilution. Tyrosine fluorescence at 302 nm was corrected with the fluorescence for a control sample (titrated in the presence of 100 μM EDTA). Experiments were repeated three times, and data points reported are an average of three trials with the error reported as the standard deviation of the trials. For the pH-dependence of Mg binding, magnesium chloride was the varied component, and a 50 mM SPG buffer system was used for pH values of 4.5−9.0. Binding curves at each pH were determined in triplicate. The values presented are the averages of the three trials, and the reported errors are the standard deviation.

Circular Dichroism Spectroscopy. The spectra of each 200 μL sample containing 100 mM SPG buffer at pH 4−9 with 5 μM enzyme were collected using a Jasco J-1100 CD spectropolarimeter with a 1 mm pathlength. Each scan analyzed was an average of three scans at 50 nm/min with a 1.00 nm bandwidth and a digital integration time (D.I.T.) of 4 s. Data were collected from 185 to 260 nm at 0.1 nm intervals.

Metal Stoichiometry Evaluated from RibB Activity. In each reaction mixture of 200 μL, the final concentration of components was 50 mM Tris-HCl (pH 7.5), 100 μM EDTA, and 1.8 mM D-Ru5P. $MgCl_2$ was titrated in successive assays in increments of 20 μM from 0 to 220 μM. The reaction was initiated by the addition of 60 μM RibB protein purified in the presence of EDTA and incubated for 1 h at room temperature. Steady-state data were calculated using the above procedure. The experiment was repeated three times, and values reported are the averages of three trials with errors reported as standard deviations.

EPR of Mn(II)/RibB. EPR samples (300 μL of the final volume) were prepared by mixing RibB, $MnCl_2$, and sugar phosphate substrate (D-Ru5P or L-Xy5P) in millimolar ratios (as defined by the experiments, *e.g.*, 3:3:3) in 50 mM Tris-HCl (pH 7.5) and 10% glycerol at 4 °C. Reactions were initiated by the addition of enzyme into the 4 mm quartz EPR tube that contained the metal and sugar phosphate components. The reaction was quenched at the specific times by submerging the EPR tube in liquid nitrogen. X-band EPR data were collected on a 9 GHz Bruker EMXPlus spectrometer. Experiments were run at 10 K with the use of an Oxford ESR900 continuous-flow liquid helium cryostat equipped with an Oxford ITC503 temperature system. Perpendicular-mode data were collected in a dual-mode Bruker ER4116DM cavity. Spectra were recorded using the following non-saturating conditions: 9.64 GHz microwave frequency, 2.0 mW microwave power, 4 G modulation amplitude, 100 kHz modulation frequency, and 40.96 ms time constant.

https://doi.org/10.1021/jacs.2c03376
J. Am. Chem. Soc. 2022, 144, 12769−12780

RibB Crystallization. All crystals were grown at room temperature using the hanging-drop vapor diffusion method. Each drop (3 μL) was prepared by mixing protein and the precipitant solution in equal amounts. Seven crystal structures are described herein [apo-RibB (7UEZ); RibB/D-Ru5P (7UF0); RibB/D-R5P/Mn (7UF1); RibB/D-Xy5P/Mn (7UF2); RibB/L-Xy5P/2Mn (7UF3); RibB/Int1/Mn (7UF4); and RibB/Int2/Mn (7UF5)]. RibB protein at 40 mg/mL was used to grow cube-shaped apo-RibB crystals using a precipitant solution of 0.1 M Na_2HPO_4/NaH_2PO_4 (pH 9.3), 16% (w/v) PEG 3350, and 0.3 M glycine that reach maximal size in three weeks. These crystals were cryoprotected with 20% PEG (w/v) 3350, 5.2 mM D-Ru5P, and 0.2 mM $MgCl_2$ and flash-cooled. The remaining structures were determined from rod-shaped crystals grown using a precipitant solution of 0.1 M lithium acetate and 12−18% (w/v) PEG 3350 and reached maximal size in 2 days. The protein concentration for crystal growth was 32.9 mg/mL, and the protein was pre-incubated with the appropriate sugar phosphate prior to drop formation (the sugar phosphate for the intermediate structures was D-Ru5P). In all cases, the sugar phosphate was at 15× molar excess, except D-R5P. In this case, flakes of D-R5P were added directly to the protein solution. In preparation for data collection, the RibB: D-R5P crystals were transferred to a precipitant solution with 4 mM $MnCl_2$ and 30% (v/v) ethylene glycol. The remaining crystals were soaked in the precipitant solution with 40 mM of a non-substrate sugar phosphate or D-Ru5P for the intermediate structures. Just before flash cooling, the crystals were transferred to a cryoprotectant solution which was the precipitant solution with 30% (v/v) ethylene glycol. For the RibB/D-Xy5P/Mn; RibB/L-Xy5P/2Mn; RibB/Int1/Mn; RibB/Int2/Mn structures, the cryoprotectant solution also contained 4 mM $MnCl_2$. For the intermediate 1 structure, the crystal remained in the second soaking solution for 3 min and for the intermediate 2 structure for 70 min.

X-ray Crystal Structure Determination. The X-ray diffraction data for all RibB crystal structures reported were collected at 100 K using the Stanford Synchrotron Radiation Laboratory (SSRL, Stanford, CA) beamlines 12−2 (apo-RibB structure) and 9−2 (all other structures). The software package Blu-Ice[30,31] was used to collect 1200 oscillation images (0.15° per image) with an exposure time of 0.2 s. The incident wavelength for the apo-RibB structure was 0.8526 Å, and for all remaining structures, it was 0.9795 Å. Data collection and refinement statistics are in Table S1. All phasing solutions were obtained by molecular replacement using PHENIX, Phaser-MR.[32] The model for the apo-RibB molecular replacement calculation was PDB:4P8J, whereas all other used 4P8E.[23] The log likelihood gain and the final translation function Z (TFZ) score for each solution are found in Table S2. Solutions were subjected to alternating cycles of model building and refinement using Coot[33] and Phenix.Refine.[34,35] Water molecules were added automatically and inspected manually using Coot. All ligands were added manually (sugar phosphates, intermediates, metals, and ethylene glycol) with restraints for the sugar phosphates generated using eLBOW[36] and REEL.[37] Anisotropic B-factors were only used for the high-resolution apo-RibB structure. The components of the final models (residues, waters, metals, and sugar phosphates) are summarized in Table S2. Structures figures were prepared using Pymol (Schrodinger).

6-Phosphogluconate Dehydrogenase (Ec6PGDH) Preparation. The overexpression construct for the *E. coli* K-12 (ATCC #47076) Ec6PGDH was prepared by GenScript. The gene was synthesized and placed into a pET-28b(+) vector, and the vector was transformed into BL21(DE3) *E. coli*. This overexpression construct yields protein with an N-terminal 6 His tag. The transformed bacteria were grown overnight at 37 °C in 100 mL of LB broth with 50 μg/mL kanamycin in a shaker incubator (250 rpm). 1L of LB broth with 50 μg/mL kanamycin was inoculated with 35 mL of the overnight culture and grown at 37 °C in a baffled flask in a shaker incubator (250 rpm). When the culture OD_{600nm} reached 0.9, protein expression was induced with a final concentration of 1 mM IPTG and was further incubated at 20 °C for overnight with shaking. The cells were harvested by centrifugation (6000*g*, 10 min, 4 °C). The cell pellet was resuspended in 10 mL of 25 mM Tris-HCl (pH 8.0), 50 mM imidazole, and 500 mM NaCl per liter of culture broth. Resuspended cells were lysed by passage through a French Press three times at 13,000 psi. The cell lysate was centrifuged at 12,000*g* for 30 min at 4 °C. The supernatant was injected onto a 25 mL Chelating Sepharose Fast Flow (GE Healthcare) column charged with nickel chloride and pre-equilibrated with 25 mM Tris-HCl (pH 8.0), 50 mM imidazole, and 500 mM NaCl. The protein was eluted with a step gradient with an imidazole concentration of 300 mM imidazole. The fractions containing the Ec6PGDH were dialyzed into 25 mM Tris-HCl (pH 8.0) and stored for later use at −80 °C. The final yield was 648 mg per liter of culture, as determined by Bradford analysis.

Preparation of ^{13}C-Labeled Ribulose 5-Phosphate. Singly and uniformly ^{13}C-labeled D-ribulose 5-phosphate was prepared by reconstitution of the pentose phosphate pathway following the published protocol.[38] In a final volume of 4 mL, 50 mM Tris-HCl (pH 7.5), 40 mM $MgCl_2$, 40 mM ATP, 37 mM labeled ^{13}C glucose (Cambridge Isotope Laboratories and Sigma), and 10 mM DTT (GoldBio) were mixed, and the pH was adjusted to 7.8 using 1 M NaOH. Hexokinase [60 U, Sigma-Aldrich, *Saccharomyces cerevisiae* (*S. cerevisiae*)] was added, and the solution was incubated at 37 °C for 30 min. In a second vial, 4 mL of 75 mM ammonium acetate, 10 mM $NADP^+$, and 70 mM α-ketoglutarate were mixed, and the pH was adjusted to 7.8 with 1 M NaOH. The two vials were combined, and 20 μM Ec6PGDH (final concentration), 20 U glutamate dehydrogenase (Sigma-Aldrich, bovine liver), and 12 U glucose 6-phosphate dehydrogenase (Sigma-Aldrich, *S. cerevisiae*) were added. The reaction was incubated at 37 °C for 3 h. Barium chloride, at a final concentration of 50 mM, was added to the solution. The solution was mixed and incubated on ice for 5 min. A white precipitate formed and was pelleted by centrifugation (4300*g*, 20 min, 4 °C). The supernatant was incubated in 80% ethanol at −20 °C for 30 min. The precipitate was washed in 90% ethanol twice and dried under nitrogen. The dried white solid was resuspended in 15 mL of water, and sodium sulfate was added to 100 mM. The white precipitate was removed by centrifugation (4300*g*, 20 min, 4 °C). The supernatant was lyophilized producing a white powder that was resuspended in 50 mM Tris-HCl (pH 8.0). The concentration of D -[^{13}C]-Ru5P was determined by colorimetric assay[18] and the standard curve using unlabeled D-Ru5P (Sigma-Aldrich), as previously described. The D-Ru5P was authenticated by ^{13}C NMR using published peak assignments.[16]

Acid-Quenched Single Turnover Monitored by NMR. RibB in 50 mM Tris-HCl (pH 8.0) was concentrated to 120 mg/mL (5.0 mM). The reaction mixture contained 50 mM Tris-HCl (pH 8.0), 20% D_2O, 3 mM $MgCl_2$, and 2.8 mM RibB. The reaction was equilibrated to 4 °C and initiated by the addition of 2 mM D -[^{13}C]-Ru5P. At specific times, 500 μL was withdrawn and quenched by the addition of 50 μL of 4 M H_2SO_4. The quenched reaction mixtures were stored in −20 °C until NMR data acquisition. All ^{13}C NMR spectra were recorded on a Bruker Avance III HD (500 MHz) equipped with a Prodigy CryoProbe at 298 K. ^{1}H decoupled ^{13}C spectra (pulse sequence: udeft) were recorded with 256 scans, a pre-acquisition delay of 4 s, and a sweep width of 240 ppm. ^{1}H coupled ^{13}C spectra (pulse sequence: zggd) were recorded with 256 or 4096 scans, a pre-acquisition delay of 3 s, and a sweep width of 250 ppm. The spectra were referenced based on the published spectra.[16]

RESULTS

RibB Production and Activity. *V. cholerae* RibB with an N-terminal histidine tag was heterologously expressed in *E. coli* and purified in two chromatographic steps, nickel affinity and gel filtration. Steady-state kinetic parameters were determined using a colorometric assay that was originally designed for high-throughput screening using the *E. coli* isozyme.The assay measures the production of terminal ketones by reacting with excess creatine and naphthol.[39,40] However, for screening, the substrate was developed *in situ* from ribose 5-phosphate using pentose phosphate isomerase to generate ribulose 5-phosphate.

https://doi.org/10.1021/jacs.2c03376
J. Am. Chem. Soc. 2022, 144, 12769−12780

We have adapted the assay such that we provide the sugar phosphate of interest directly, using dihydroxybutanone to generate a standard curve for quantitation. The assay yielded kinetic parameters when D-Ru5P was used as the varied substrate, k_{cat} = 2.2 ± 0.2 min^{-1}; K_m = 277 ± 3 μM; and k_{cat}/K_m = 130 ± 10 $M^{-1}s^{-1}$. When Mg^{2+} was the varied component, k_{cat} = 2.7 ± 0.4 min^{-1}; K_m = 70 ± 10 μM; and k_{cat}/K_m = 600 ± 200 $M^{-1}s^{-1}$. When Mn^{2+} was substituted for Mg^{2+} as the varied component, k_{cat} = 0.7 ± 0.1 min^{-1}; K_m = 11 ± 1 μM; and k_{cat}/K_m = 1050 ± 20 $M^{-1}s^{-1}$. This represents an almost two-fold increase in the catalytic efficiency for Mn^{2+} compared to Mg^{2+}. The Michaelis−Menten plots are found in Figure S1.

RibB is a Mononuclear Metal Enzyme. RibB is reported to be a Mg-dependent enzyme, and crystal structures with a variety of metals bound (Mg^{2+}, Zn^{2+}, and Ca^{2+}) show two metal ions in the active site (Figure 2). For this reason, proposed chemical mechanisms have assumed the involvement of two Mg^{2+} ions.[20,21,23,27] To test this assumption, RibB was titrated with metals (Mg^{2+}, Zn^{2+}, and Mn^{2+}) against a known concentration of enzyme (60 μM), and metal binding was measured by intrinsic tyrosine fluorescence. Because adventitious metals from protein production and purification were difficult to remove, the protein was purified in the presence of 100 μM EDTA, and all buffers for these experiments contained 100 μM EDTA. Therefore, assuming EDTA has a higher affinity for the added metal ions than RibB, a change in fluorescence is expected once the metal concentration exceeds 100 μM, and the change should come to a limit once sufficient metal is bound that the tyrosine environment is no longer changing appreciably. The titration experiment shows that tyrosine fluorescence begins increasing once 100 μM metal is added (the EDTA is saturated) and appears to saturate at ∼160 μM (equivalent to the EDTA concentration added to the protein concentration), keeping in mind the large error of this low signal assay. In other words, one equivalent of metal saturates the change in the signal (Figure 3A). A similar titration was performed measuring activity instead of tyrosine fluorescence. Activity assay confirms that RibB is inactive in the presence of Zn^{2+} but active in the presence of Mg^{2+} and Mn^{2+} and shows that no more than one metal ion is required for full activity (Figure 3B). One would be tempted to propose that additional Mn^{2+} ions over 1:1 ratio was inhibitory; however, after the addition of one equivalent of Mn^{2+}, enzyme precipitation is observed, which is the likely cause of the decrease in the activity above 160 μM Mn^{2+}. Mn^{2+} has also been reported to interfere with the color development in assay.[18]

Before discussing the EPR spectra for this present system, we briefly summarize prior relevant EPR studies of Mn-substituted dinitrogenase reductase. When subjected to EPR, di-nuclear Mn^{2+} center of dinitrogenase reductase shows characteristic sets of ^{55}Mn hyperfine lines at 2800G and 3800G with hyperfine splitting of 45G. However, the spectra also reveal a high intensity six peak pattern at 3400G suggestive of free Mn^{2+} metal ions in solution (*i.e.*, hexa-aqua Mn^{2+}).[41] Following a similar methodology, we first mixed D-Ru5P with Mn^{2+}: the spectra showed the high intensity pattern expected for free Mn^{2+} (black trace, Figure 4). RibB with an equimolar concentration of Mn^{2+} showed the same six peak pattern but at significantly lowered intensity, indicating binding of Mn^{2+} to the protein (blue trace). Equimolar RibB and Mn^{2+} (3 mM) were mixed with catalytically inactive substrate analogue L-Xy5P (2 mM) and incubated for 10 min before being freeze-quenched. This spectrum shows hyperfine splitting of 46G at 2800G and 4000G, characteristic of a di-Mn^{2+} center (dark red trace). As we will see in the crystal structures described below, the L-Xy5P structure has a di-Mn^{2+} center. Finally, equimolar RibB and Mn^{2+} (3 mM) were mixed with substrate D-Ru5P (2 mM) and incubated for 10 min (approximately two half-lives of the k_{cat} value or 75% complete) before being quenched by freezing. Note the characteristic six peak pattern at 3400G suggestive of metal binding within the enzyme (gold trace),

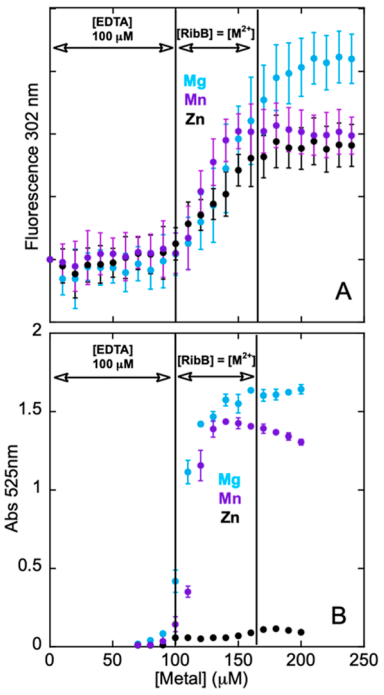

Figure 3. RibB is a mononuclear metal enzyme by binding and activity assays. (A) Intrinsic tyrosine fluorescence shows a 1:1 stoichiometry of metal/RibB for Mg(II), Zn(II), or Mn(II), once the concentration of EDTA is surpassed. (B) Activity assays show one equivalent of Mg(II) or Mn(II) is required for full activity, and that Zn(II) is noncatalytic. [RibB] = 60 μM, [EDTA] = 100 μM.

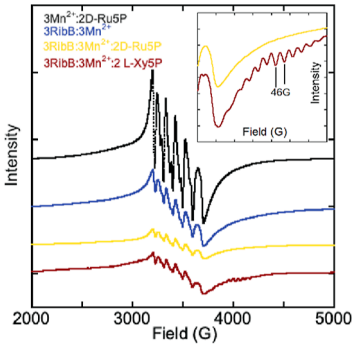

Figure 4. RibB is a mononuclear metal enzyme by EPR. EPR samples were prepared by mixing RibB, $MnCl_2$, and sugar phosphate substrate (D-Ru5P or L-Xy5P) in the millimolar ratios shown. The enzyme was added as the final component, and the reaction was quenched by freezing in liquid nitrogen after a 10 min incubation. The non-substrate sugar phosphate L-Xy5P sample shows the characteristic hyperfine splitting for a di-manganese center (inset, dark red), whereas the substrate D-Ru5P sample does not exhibit this feature (gold) indicating only one metal in the catalytic site for turnover.

https://doi.org/10.1021/jacs.2c03376
J. Am. Chem. Soc. 2022, 144, 12769−12780

without hyperfine splitting below 3200G, indicating one Mn^{2+} in the active complex.

RibB Catalysis is pH Dependent. RibB shows a significant decrease in steady-state kinetic parameters at pH values below pH 7, leading to the initial hypothesis that a catalytic base could be important in the mechanism (Figure 5A). To ensure that the pH dependence of catalytic activity

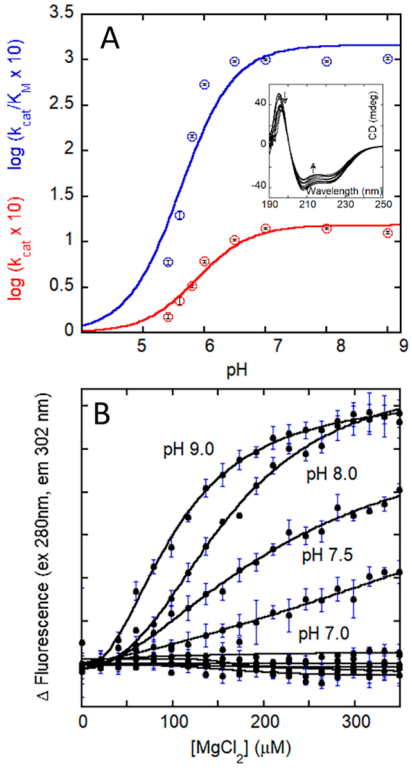

Figure 5. RibB shows a pH dependence for catalytic activity that is associated with the binding of the catalytically required magnesium ion. (A) Steady-state kinetic parameters show a significant decrease in activity at pH values below 7. Inset. RibB maintained a primarily α-helical structure from pH 4 to pH 9, arrows indicate trend with increasing pH. (B) Catalytically required metal only binds to the protein at pH values above pH 6.

was not merely a function of protein folding, circular dichroism spectra were measured from pH 4 to 9, showing that the protein retained a predominantly α-helical fold at all pH values (Figure 5A inset). Magnesium ion-binding isotherms across the same pH range using the tyrosine fluorescence assay showed that the metal ion binds to the enzyme with high affinity at pH values above 7 (Figure 5B). Therefore, the catalytic dependence, as shown in Figure 5A, is associated with the protein's ability to bind the catalytically required magnesium ion. Since the magnesium ion is coordinated by His154, it is tempting to speculate that the pH effect is due to the deprotonation of this residue, providing a lone pair of electrons for metal ion coordination.

Active and Inactive Metal−Substrate Complexes in the RibB Active Site. The enzymatic activity of RibB with different 5-carbon sugar phosphates was compared with their binding modes in the active site. First, the apo-RibB structure was determined to very high resolution (1.08 Å). A representative electron density map is found in Figure S2. The RibB active site is enclosed by two mobile loops. Residues 33−42 comprise Loop 1, which contains Glu39. In the apo-structure, Loop 1 is in an open conformation, with Glu39 pointing away from the active site, unavailable to chelate the metal ion required for catalysis. Residues 83−97 comprise Loop 2, which is disordered in this structure. A second metal ion chelating residue, His154, is the terminal residue of a helix composed of residues 154−165. This secondary structural element holds the backbone of His154 in place but without sugar phosphate or metal or closed loops 1 and 2, and the side chain has a rotameric conformation that differs from that observed for all other structures solved (Figure 6A).

The structure of RibB was determined with the biological substrate D-ribulose 5-phosphate in the absence of a metal ion (RibB/D-Ru5P; Figure 6B). D-Ru5P binds in an extended conformation similar to that seen in the reported D-Ru5P:2Zn structure, as shown in Figure 2. Both loops 1 and 2 are in their closed conformations in this structure, and Glu39 and His154 are positioned for metal chelation. Crystals of this kind were soaked with Mn^{2+} for the structures of the reaction intermediates, described below. As noted above (and for easy comparison here), when magnesium ions are added, RibB demonstrates a K_m = 277 ± 3 μM with D-Ru5P. Ribose 5-phosphate (D-R5P) is the aldopentose analogue of the ketopentose biological substrate ribulose 5-phosphate (D-Ru5P). D-R5P is a poor substrate for RibB, with a K_m estimated to be 25−50 mM (Figure S1B, blue). The data do not fit to a Michaelis−Menten model due to significant inhibition at higher concentrations of the substrate. A crystal structure with the sugar phosphate shows a binding mode similar to D-Ru5P and can be trapped in the presence of manganese, chelated as expected in the active site by Glu-39 and His-154 (Figure 6C). The aldopentose D-xylulose 5-phosphate (D-Xy5P) is a better substrate (K_m estimated at 2−3 mM) but with a similar inhibition profile to D-R5P (Figure S1A, dark red). The structure of RibB with Mn^{2+} and D-Xy5P was determined and is shown in Figure 6D. This sugar phosphate binds in a more elongated pose with the hydroxyls of C3 and C4 in an alternate conformation than seen in D-Ru5P and D-R5P, due to the change in chirality at C3. Finally, the structure was determined with the aldopentose L-xylulose 5-phosphate (L-Xy5P), showing two manganese ions and a significantly different, more twisted binding mode (Figure 6E). This sugar phosphate showed no activity at any concentration tested.

Assignment of NMR Spectra of Acid-Quenched RibB D-Ru5P Reactions. The exceptionally slow turnover number of VcRibB at 4 °C provided the opportunity to halt the reaction at specific times and analyze the reaction mixture in a time-dependent manner. The quenched samples were analyzed using ^{13}C NMR for both fully labeled D-Ru5P and repeated using substrate singly labeled at each carbon. Figure 7 depicts representative ^{1}H decoupled ^{13}C NMR resonances of the substrate, products, and two distinct reaction states and as such do not represent discrete reaction times.

In this figure, the resonances of individual carbons are color-coded so that the reaction path traversed, and destination of individual carbons is apparent. Overlayed in gray are the ^{1}H decoupled ^{13}C NMR resonances observed for the fully ^{13}C-labeled substrate. All NMR spectra including ^{1}H spectra for singly ^{13}C-labeled substrates collected are shown in Figures S3−S12. The assignment based on these spectra are summarized at the right in Figure 7, and the ^{1}H decoupled-^{13}C resonances and multiplicities for the four reaction states observed are listed in Table S3. Definitive assignment of the

https://doi.org/10.1021/jacs.2c03376
J. Am. Chem. Soc. 2022, 144, 12769−12780

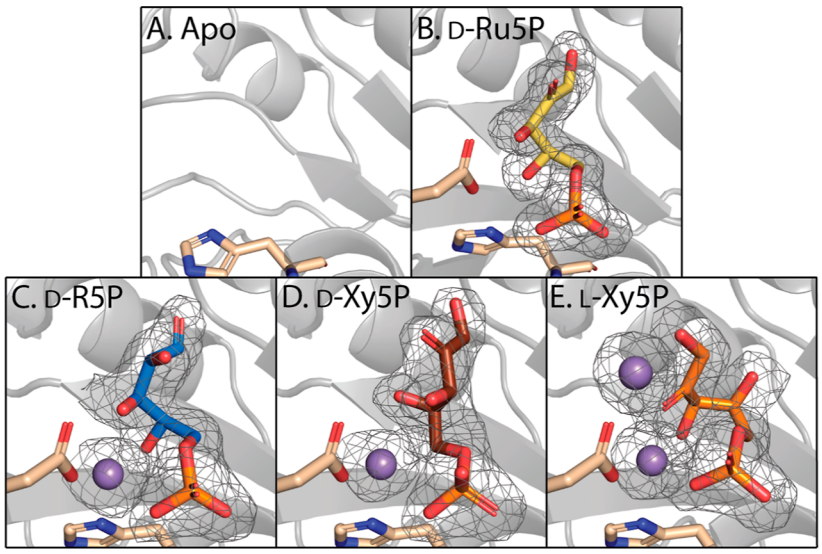

Figure 6. Structures of RibB with sugar phosphates that are substrate analogues show only one metal ion in the active site, and the sugar phosphates bind in an elongated fashion. The RibB structure with a variety of sugar phosphate molecules with metal coordinating residues, Glu39 and His154 shown as wheat colored. (A) RibB was crystallized in the absence of sugar phosphate in an open conformation such that the active site loop containing Glu39 coordinating the metal ion is not visible in this image. (B) Addition of D-Ru5P (yellow sticks) to the crystal orders the active site loop of RibB with an extended conformation of the sugar phosphate, as seen in previous structures. The substrates (C) D-R5P (blue) and (D) D-Xy5P (dark red) have the sugar phosphates in a similar elongated conformation and contain one Mn^{2+} ion in the active site. (E) L-Xy5P (orange) is not a substrate for RibB and binds in the active site in a twisted conformation and coordinates two Mn^{2+} metals. Manganese ions are depicted as purple spheres. The maps are Polder maps contoured at 3 σ.[42]

progression for each carbon was made from the singly ^{13}C-labeled substrates (Figures S3−S8); these data show two intermediate states accumulate and decay between 0 and 5 min. Conversion of C1 from an alcohol to a primary alkyl state is observed as a 40 ppm upfield shift which is retained as the molecule is converted to a subsequent intermediate before resolving to the product. In contrast, C2 retains a resonance consistent with a ketone throughout the reaction. In the progression from D-Ru5P to intermediate 1, C3 moves ∼22 ppm downfield to a chemical shift of 96.2 ppm indicative of a gem-diol carbon. This is interpreted as a hydration artifact arising from acid quench and indicates that C3 is likely a carbonyl in the first transient observed. The resonance for this carbon moves upfield in the subsequent intermediate state, revealing its return to an alcohol state, and this state is retained in the DHBP product. C4 resonates as a hydroxyl bearing carbon in both the substrate and intermediate 1 states but moves downfield to resonate as a gem-diol in the second transient species to then resolve as a formate carboxylate in the spectrum of the products. For the species observed, the chemical nature of C5 does not change and thus resonates within a 2 ppm range throughout the reaction and moreover exhibits a consistent small 4−5 Hz coupling to the two-bond distant ^{31}P of the phosphate moiety. The transient species observed clearly indicate the accumulation and decay of two intermediate states in single turnover of VcRibB. Neither of the assigned states definitively identify a single species but are each consistent with acid quench of two successive states, shown as boxed in Figure 1.

Remarkably, the same two intermediate states are observed by X-ray crystallography. Crystals grown with the substrate D-Ru5P were soaked for 3 min in a cryo-protectant solution containing Mn^{2+} before being plunged in liquid nitrogen to stop the reaction and prepare the crystal for diffraction. When this structure was solved, the density of the closed active site is best modeled to contain 80% substrate (D-Ru5P) and 20% of intermediate 1, with the 2-keto, 3,3-diol (Figure 7B) produced by the acid quench NMR experiment, more accurately depicted as a 2,3-diketone (Figure 8A). Crystals soaked for 70 min in the Mn^{2+}-containing cryo-protectant display density consistent with 56% Intermediate 2 that was modeled as the gem-diol. While the acid quench NMR data are consistent with hydration by the enzyme to make the gem diol, it is also possible that the acid quench performed the hydration of the preceding aldehyde intermediate (Figure 1). However, the crystallographic data shows density consistent with the C4 gem diol (Figures 1 and 7C). This intermediate is modeled as the predominant fraction of the density and has the sp^3 C3 somewhat flattened. This geometry is suggestive of strain that would facilitate formate elimination and formation of the trigonal planar C3 enol of the DHBP tautomer (Figure 1). The remaining 44% of the density was fit to the two products, dihydroxybutanone phosphate and formate (Figure 8B).

DISCUSSION

The identity of the four-carbon unit required in the condensation of 5-amino-6-ribitylamino-2,4-pyrimidinedione to form the xylene moiety of 6,7-dimethyl-8-ribityllumazine in the biosynthesis of riboflavin was a long-standing matter of conjecture. In the mid-1950s, Plaut and Broberg demonstrated that the xylene methyl groups and the carbons to which they were attached were derived from the C1 and C6 of glucose.[43,44] Later intermediates of the butanediol pathway were implicated,[45,46] and then, the pentose phosphate pathway before both were rejected.[47] Dismutation of the 5-amino-6-ribitylamino-2,4-pyrimidinedione ring was also proposed, in which the ribityl was the source of the four carbons.[48,49] Eventually, Alworth and co-workers identified the origin of the methyl groups in the 5,6-dimethylbenzimidazole moiety of cobalamin as derived from ribose-5-phosphate and given that

https://doi.org/10.1021/jacs.2c03376
J. Am. Chem. Soc. 2022, 144, 12769−12780

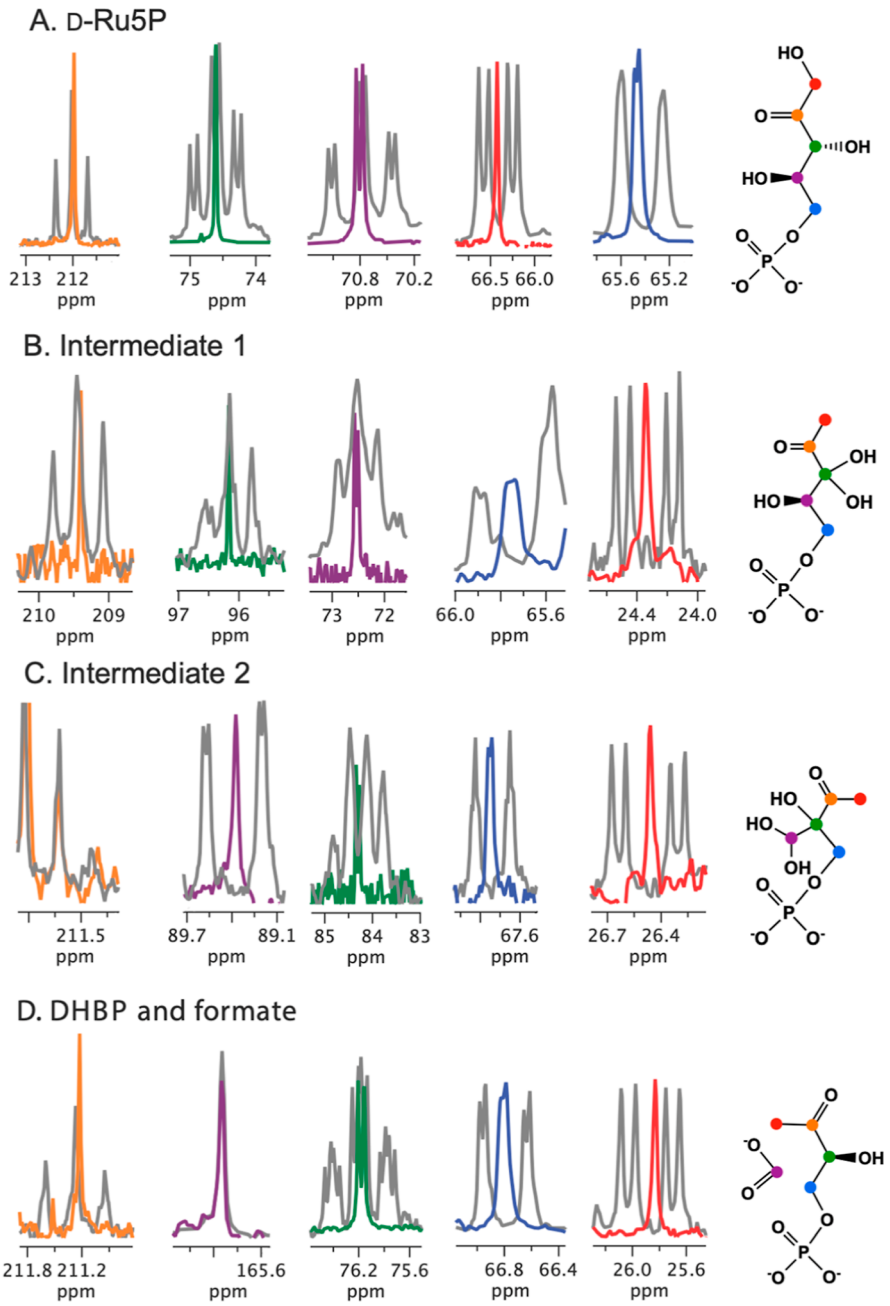

Figure 7. Identification of two reaction intermediates by single turnover NMR. RibB was followed as a single turnover reaction using ^{13}C D-Ru5P and quenched with acid at various time points. The D-Ru5P is converted to DHBP and formate with the transient appearance of two distinct intermediates. Fully labeled ^{13}C (gray) and each singly labeled carbon were followed through the reaction and shown in colors; C1 (red), C2 (orange), C3 (green), C4 (purple), and C5 (blue).

the origin of this moiety is from riboflavin, pentose sugar phosphates were again implicated as the source of the four carbons.[50−55] This proposal was later confirmed using ^{13}C labeling that also revealed that the C6-methyl, C6, and C7 came from C1−C3 of pentoses but oddly, the C7-methyl came from pentose C5.[12,13,56,57] This was the first evidence that a rearrangement reaction was required. In 1985, an activity was identified that formed a 4-carbon product that was a substrate for lumazine synthase, at last quelling prior notions that a pentose was the substrate.[58] Ultimately, D-ribulose 5-phosphate was recognized as the substrate for this newly identified enzyme, and the ^{13}C-labeled substrate was used to show that formate and L-3,4-dihydroxy-2-butanone-4-phosphate were the products,[15] putting to rest a 35-year biochemical enigma.

Soon after establishment of the reaction, a mechanism was proposed, in which the skeletal rearrangement of D-ribulose 5-phosphate was achieved via an anionotropic 1,2-migration such that the C5 attacks the pentose C3, instigating the elimination of C4 as a formate via a gem diol moiety (Figure 1).[16] This soundly reasoned mechanism was consistent with labeling and incorporation studies that show solvent deuterium incorporation at C1 and C3. The canonical mechanism has been rewritten in numerous articles since its initial proposal[20,21,23,59,60] and once the first structures of RibB were

https://doi.org/10.1021/jacs.2c03376
J. Am. Chem. Soc. 2022, 144, 12769−12780

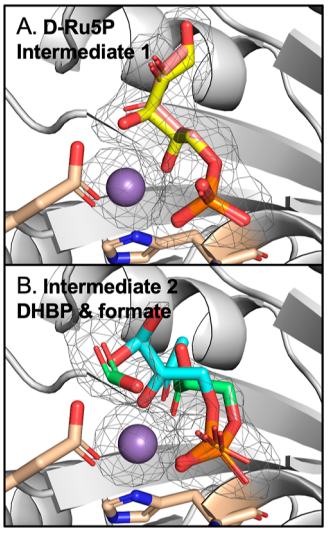

Figure 8. Identification of two reaction intermediates by single turnover X-ray crystallography. (A) RibB crystals were grown with D-ribulose 5-phosphate and soaked with $MnCl_2$ for 3 min. The map is best modeled with 80% substrate (yellow) and 20% Intermediate 1 as the 2,3-diketone (pink). (B) Crystals soaked for 70 min produced a structure with density that is modeled as 56% intermediate 2 in the gem diol form (cyan) and 44% of the two products, dihydroxybutanone phosphate and formate (green). Both structures show a single manganese ion in the active site (purple). The maps are Polder maps contoured at 3σ.

published, the mechanistic proposal has been redrawn in the context of the active site residues.[20,28]

These initial X-ray crystal structures were of RibB reconstituted with Mg, Mn, or Zn ions and revealed either one or two metal ions within the active site.[19−21,27] Contextual chemical mechanisms have generally incorporated two metal ions, and this cofactor set has become the accepted native active site configuration. Within RibB, the second metal ion has only two direct coordinating contacts, one with the substrate C2 carbonyl and one with Glu39. In contrast, the metal ion liganded to the substrate C3 and C4 hydroxyl groups, and the terminal phosphate of D-Ru5P is also coordinated to His154 and Glu39 (VcRibB residue numbers).[21] In each case, the structures solved with two metal ions were either of a vestigial, non-active form of RibB or were solved when liganded to substrate analogue sugar phosphates and so do not depict a native state of the enzyme. Moreover, in each case, when the chemical mechanism of RibB has been presented, it has rightly been described as hypothetical as little direct evidence for the chemical species involved in the reaction was available. We present the first direct evidence for the mechanism of RibB. These data show that the general reasoning of the canonical mechanism by Bacher *et al.* holds, but that it is achieved with the involvement of a single active site metal ion.

The slow turnover rate of VcRibB facilitated acid quench of the reaction, and selective ^{13}C-labeling of D-Ru5P via reconstitution of the pentose phosphate pathway gave the means for unambiguous assignment of the origin and destination of all carbons that constitute two transient species observed to accumulate under single turnover conditions (Figure 7). These data indicate elimination of the C1-hydroxyl from an ene-diol species to form a 2,3-diketone that is observed to accumulate with acid quench in the hydrated 2-keto, 3,3-diol state (Figure 9). With regard to the chemical mechanism, this localizes the quenched intermediate to either the 1-ene-2-ol-3-one species or the ensuing 2,3-diketone. The subsequent transient liberated in acid quench is the result of rearrangement and has the C5 bonded to C3 with C4 as a gem diol that is poised for elimination as formate. This is the first observation of this fundamental RibB transient, and confirmation of its existence arguably dictates much of the preceding and subsequent chemistry in the RibB catalytic cycle.

One primary role of the magnesium (or manganese) ion in RibB is Lewis acidity, stabilizing hydroxide states of coordinated hydroxyls and waters, thereby inducing tautome-

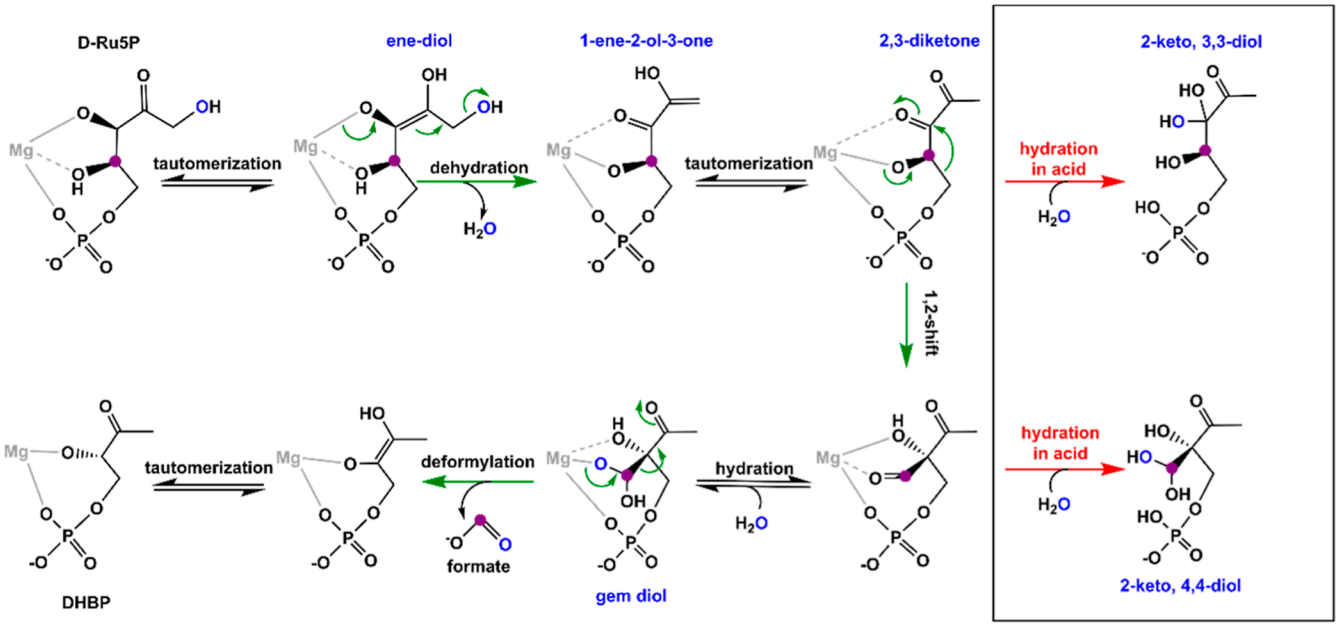

Figure 9. Evidence-based mechanism. Boxed reactions indicate hydrated acid-quenched products identified in the NMR data.

https://doi.org/10.1021/jacs.2c03376
J. Am. Chem. Soc. 2022, 144, 12769−12780

rizations, hydration, and two elimination reactions. It is not immediately apparent that a second metal ion is required to accomplish this chemistry, and each structure of VcRibB solved with a substrate or intermediate state bound that we present here has only one metal ion, and full activity is achieved with equimolar Mg or Mn (Figure 5). While this observation does not rule out transient involvement of a rapidly exchanging second metal ion amid relative slow chemistry, it does indicate that one metal ion has a dominant role and anchors substrate binding and much of the catalytic cycle. In Figure 8, we show density for a single metal ion in two states of catalysis representative of four distinct species, modeled as a 4:1 ratio of the ES complex and the 2,3-diketone intermediate (intermediate 1), and the rearranged and hydrated intermediate (intermediate 2) added to a roughly equal fraction of the product complex.

Structures of VcRibB with the native substrate, D-Ru5P, were solved in the presence of Mn ions that induce even slower rates of turnover (Figure 8). The structure of the VcRibB·Mn·D-Ru5P complex has the metal ion coordinated to the C3 and C4 hydroxyl substituents and the phosphate of the substrate. Within a 3 min incubation period, the reaction advances in crystallo to partial elimination of the C2-hydroxyl retaining coordination to the same oxygen atoms presumably with the C3 now in the keto state and the tautomeric state of the C1−C2 enol/keto group unknown. The observed conformation of intermediate 1 when best fit to the available density at 2.2 Å resolution indicates a Bürgi−Dunitz angle within 10° of optimal for the nucleophilic attack of C5 on C3. This conformation has an altitude 117° and an azimuth 145° across a gap of 2.4 Å,[61] a geometry that promotes the migration reaction that forms intermediate 2 (Figure 8A). The exact mechanism of migration is not apparent from these data. Shifts of this type are analogous to Pinacol rearrangements where migration is induced by an adjacent carbonium ion.[62] At this stage of catalysis, the Lewis acidity of the metal ion of RibB presumably works to denude the C3 carbonyl carbon of electrons increasing its electrophilicity. Whether the migration is concerted and involves a single transition state with partial bonding of C5 to both C4 and C3 or stepwise with the formation of a C5 carbanion is a nuanced chemical argument that is beyond the reach of the data presented. However, the first definitive observation of the predicted migration product (intermediate 2) confines the mechanistic possibilities considerably and confirms an otherwise unsubstantiated mechanism first proposed in 1991.[16]

The crystallographic intermediate 2 state, as shown in Figure 8B, has density for the C4 gem diol. This is therefore the same as the species observed as the second transient in acid quench NMR data (Figure 7), indicating that the decay of the gem diol to form formate and the enol form of the DHBP product is the rate-limiting chemical step. The product complex includes density for formate and DHBP and is the first experimental observation of these products formed *in situ*.

CONCLUSIONS

Thirty-one years after the initial hypothetical chemical mechanism for RibB was offered, definitive evidence for the accumulation, decay, and chemical identity of two sequential transients is presented. These data indicate that the fundamental steps of 1,2-shift of carbon-five and formate elimination from a gem diol bonded to a quaternary carbon-three define the salient and unique catalytic steps of the enzyme's catalytic cycle.

ASSOCIATED CONTENT

Supporting Information

The Supporting Information is available free of charge at https://pubs.acs.org/doi/10.1021/jacs.2c03376.

Additional crystallographic details; steady-state kinetics; NMR time-course data; proton-coupled NMR data; chemical shifts; and coupling constants for intermediate states (PDF)

AUTHOR INFORMATION

Corresponding Author

Audrey L. Lamb − *Department of Molecular Biosciences, University of Kansas, Lawrence, Kansas 66045, United States; Department of Chemistry, University of Texas at San Antonio, San Antonio, Texas 78249, United States;* orcid.org/0000-0002-2352-2130; Email: audrey.lamb@utsa.edu

Authors

Nikola Kenjić − *Department of Molecular Biosciences, University of Kansas, Lawrence, Kansas 66045, United States;* orcid.org/0000-0002-2871-7674

Kathleen M. Meneely − *Department of Molecular Biosciences, University of Kansas, Lawrence, Kansas 66045, United States; Department of Chemistry, University of Texas at San Antonio, San Antonio, Texas 78249, United States;* orcid.org/0000-0002-0372-9695

Daniel J. Wherritt − *Department of Chemistry, University of Texas at San Antonio, San Antonio, Texas 78249, United States;* orcid.org/0000-0002-8616-9864

Melissa C. Denler − *Department of Chemistry, University of Kansas, Lawrence, Kansas 66045, United States;* orcid.org/0000-0003-2443-6178

Timothy A. Jackson − *Department of Chemistry, University of Kansas, Lawrence, Kansas 66045, United States;* orcid.org/0000-0002-3529-2715

Graham R. Moran − *Department of Chemistry and Biochemistry, University of Loyola, Chicago, Illinois 60660, United States;* orcid.org/0000-0002-6807-1302

Complete contact information is available at: https://pubs.acs.org/10.1021/jacs.2c03376

Funding

This publication was made possible by funds from NIH Grants R01 GM127655 and NSF grant 1904494/2041047 to A.L.L. and the University of Kansas General Research Fund. G.R.M. was supported by NSF Grant 1904480 and the Loyola University College of Arts and Sciences. N.K. was supported by the Weaver International Fellowship. M.C.D. was supported by the National Institutes of Health Graduate Training Program in the Dynamic Aspects of Chemical Biology (T32 GM008545). The content is solely the responsibility of the authors and does not necessarily represent the official views of the National Institute of General Medical Sciences or the National Institutes of Health.

Notes

The authors declare no competing financial interest.

■ ACKNOWLEDGMENTS

Use of the Stanford Synchrotron Radiation Lightsource, SLAC National Accelerator Laboratory, is supported by the U.S. Department of Energy, Office of Science, Office of Basic Energy Sciences under Contract DE-AC02-76SF00515. The Stanford Synchrotron Radiation Lightsource Structural Molecular Biology Program is supported by the U.S. Department of Energy Office of Biological and Environmental Research and by NIGMS, the National Institutes of Health Grant P41GM103393. We thank the staff at the Stanford Synchrotron Radiation Laboratory for their support and assistance. We are grateful to Justin T. Douglas and Sarah A. Neuenswander of the University of Kansas NMR facility for support and assistance. The authors would also like to express thanks to James Devery of the Loyola University Chicago for helpful discussions regarding rearrangement mechanisms.

■ REFERENCES

(1) Thakur, K.; Tomar, S. K.; Singh, A. K.; Mandal, S.; Arora, S. Riboflavin and health: A review of recent human research. *Crit. Rev. Food Sci. Nutr.* **2017**, *57*, 3650−3660.

(2) Bacher, A.; Eberhardt, S.; Fischer, M.; Kis, K.; Richter, G. Biosynthesis of vitamin B2 (riboflavin). *Annu. Rev. Nutr.* **2000**, *20*, 153−167.

(3) Powers, H. J.; Weaver, L. T.; Austin, S.; Beresford, J. K. A proposed intestinal mechanism for the effect of riboflavin deficiency on iron loss in the rat. *Br. J. Nutr.* **1993**, *69*, 553−561.

(4) Thiagarajan, V.; Byrdin, M.; Eker, A. P. M.; Müller, P.; Brettel, K. Kinetics of cyclobutane thymine dimer splitting by DNA photolyase directly monitored in the UV. *Proc. Natl. Acad. Sci. U.S.A.* **2011**, *108*, 9402−9407.

(5) Lakshmi, R.; Lakshmi, A. V.; Divan, P. V.; Bamji, M. S. Effect of riboflavin or pyridoxine deficiency on inflammatory response. *Indian J. Biochem. Biophys.* **1991**, *28*, 481−484.

(6) Schramm, M.; Wiegmann, K.; Schramm, S.; Gluschko, A.; Herb, M.; Utermöhlen, O.; Krönke, M. Riboflavin (vitamin B2) deficiency impairs NADPH oxidase 2 (Nox2) priming and defense against *Listeria monocytogenes*. *Eur. J. Immunol.* **2014**, *44*, 728−741.

(7) Long, Q.; Ji, L.; Wang, H.; Xie, J. Riboflavin biosynthetic and regulatory factors as potential novel anti-infective drug targets. *Chem. Biol. Drug Des.* **2010**, *75*, 339−347.

(8) Sassetti, C. M.; Boyd, D. H.; Rubin, E. J. Genes required for mycobacterial growth defined by high density mutagenesis. *Mol. Microbiol.* **2003**, *48*, 77−84.

(9) Mack, M.; Grill, S. Riboflavin analogs and inhibitors of riboflavin biosynthesis. *Appl. Microbiol. Biotechnol.* **2006**, *71*, 265−275.

(10) Bacher, A.; Le Van, Q.; Buhler, M.; Keller, P.J.; Eimicke, V.; Floss, H. G. Biosynthesis of riboflavin. Incorporation of D-[1^{-13}C]Ribose. *J. Am. Chem. Soc.* **1982**, *104*, 3753−3755.

(11) Bacher, A.; Le Van, Q.; Keller, P. J.; Floss, H. G. Biosynthesis of riboflavin. Incorporation of ^{13}C-labeled precursors into the xylene ring. *J. Biol. Chem.* **1983**, *258*, 13431−13437.

(12) Bacher, A.; Le Van, Q. L.; Keller, P. J.; Floss, H. G. Biosynthesis of riboflavin. Incorporation of multiple ^{13}C-labeled precursors into the xylene ring. *J. Am. Chem. Soc.* **1985**, *107*, 6380−6385.

(13) Le Van, Q.; Keller, P. J.; Bown, D. H.; Floss, H. G.; Bacher, A. Biosynthesis of riboflavin in *Bacillus subtilis*: origin of the four-carbon moiety. *J. Bacteriol.* **1985**, *162*, 1280−1284.

(14) Volk, R.; Bacher, A. Biosynthesis of riboflavin. The structure of the four-carbon precursor. *J. Am. Chem. Soc.* **1988**, *110*, 3651−3653.

(15) Volk, R.; Bacher, A. Studies on the 4-carbon precursor in the biosynthesis of riboflavin. Purification and properties of L-3,4-dihydroxy-2-butanone-4-phosphate synthase. *J. Biol. Chem.* **1990**, *265*, 19479−19485.

(16) Volk, R.; Bacher, A. Biosynthesis of riboflavin. Studies on the mechanism of L-3,4-dihydroxy-2-butanone 4-phosphate synthase. *J. Biol. Chem.* **1991**, *266*, 20610−20618.

(17) Kelly, M. J. S.; Ball, L. J.; Krieger, C.; Yu, Y.; Fischer, M.; Schiffmann, S.; Schmieder, P.; Kühne, R.; Bermel, W.; Bacher, A.; Richter, G.; Oschkinat, H. The NMR structure of the 47-kDa dimeric enzyme 3,4-dihydroxy-2-butanone-4-phosphate synthase and ligand binding studies reveal the location of the active site. *Proc. Natl. Acad. Sci. U.S.A.* **2001**, *98*, 13025−13030.

(18) Picollelli, M. A.; Viitanen, P. V.; Jordan, D. B. Spectrophotometric determination of 3, 4-dihydroxy-2-butanone-4-phosphate synthase activity. *Anal. Biochem.* **2000**, *287*, 347−349.

(19) Liao, D.-I.; Calabrese, J. C.; Wawrzak, Z.; Viitanen, P. V.; Jordan, D. B. Crystal structure of 3,4-dihydroxy-2-butanone 4-phosphate synthase of riboflavin biosynthesis. *Structure* **2001**, *9*, 11−18.

(20) Liao, D.-I.; Zheng, Y.-J.; Viitanen, P. V.; Jordan, D. B. Structural definition of the active site and catalytic mechanism of 3,4-dihydroxy-2-butanone-4-phosphate synthase. *Biochemistry* **2002**, *41*, 1795−1806.

(21) Steinbacher, S.; Schiffmann, S.; Richter, G.; Huber, R.; Bacher, A.; Fischer, M. Structure of 3,4-dihydroxy-2-butanone 4-phosphate synthase from *Methanococcus jannaschii* in complex with divalent metal ions and the substrate ribulose 5-phosphate: implications for the catalytic mechanism. *J. Biol. Chem.* **2003**, *278*, 42256−42265.

(22) Varadi, M.; Berrisford, J.; Deshpande, M.; Nair, S. S; Gutmanas, A.; Armstrong, D.; Pravda, L.; Al-Lazikani, B.; Anyango, S.; Barton, G. J; et al. PDBe-KB a community-driven resource for structural and functional annotations. *Nucleic Acids Res.* **2020**, *48*, D344−D353.

(23) Islam, Z.; Kumar, A.; Singh, S.; Salmon, L.; Karthikeyan, S. Structural basis for competitive inhibition of 3,4-dihydroxy-2-butanone-4-phosphate synthase from *Vibrio cholerae*. *J. Biol. Chem.* **2015**, *290*, 11293−11308.

(24) Singh, M.; Kumar, P.; Yadav, S.; Gautam, R.; Sharma, N.; Karthikeyan, S. The crystal structure reveals the molecular mechanism of bifunctional 3,4-dihydroxy-2-butanone 4-phosphate synthase/GTP cyclohydrolase II (Rv1415) from *Mycobacterium tuberculosis*. *Acta Crystallogr., Sect. D: Biol. Crystallogr.* **2013**, *69*, 1633−1644.

(25) Liao, D. I.; Viitanen, P. V.; Jordan, D. B. Cloning, expression, purification and crystallization of dihydroxybutanone phosphate synthase from *Magnaporthe grisea*. *Acta Crystallogr., Sect. D: Biol. Crystallogr.* **2000**, *56*, 1495−1497.

(26) Steinbacher, S.; Schiffmann, S.; Bacher, A.; Fischer, M. Metal sites in 3,4-dihydroxy-2-butanone 4-phosphate synthase from *Methanococcus jannaschii* in complex with the substrate ribulose 5-phosphate. *Acta Crystallogr., Sect. D: Biol. Crystallogr.* **2004**, *60*, 1338−1340.

(27) Kumar, P.; Singh, M.; Gautam, R.; Karthikeyan, S. Potential anti-bacterial drug target: structural characterization of 3,4-dihydroxy-2-butanone-4-phosphate synthase from *Salmonella typhimurium* LT2. *Proteins* **2010**, *78*, 3292−3303.

(28) Echt, S.; Bauer, S.; Steinbacher, S.; Huber, R.; Bacher, A.; Fischer, M. Potential anti-infective targets in pathogenic yeasts: structure and properties of 3,4-dihydroxy-2-butanone 4-phosphate synthase of *Candida albicans*. *J. Mol. Biol.* **2004**, *341*, 1085−1096.

(29) Newman, J. Novel buffer systems for macromolecular crystallization. *Acta Crystallogr., Sect. D: Biol. Crystallogr.* **2004**, *60*, 610−612.

(30) McPhillips, T. M.; McPhillips, S. E.; Chiu, H.-J.; Cohen, A. E.; Deacon, A. M.; Ellis, P. J.; Garman, E.; Gonzalez, A.; Sauter, N. K.; Phizackerley, R. P.; Soltis, S. M.; Kuhn, P. Blu-Ice and the Distributed Control System: software for data acquisition and instrument control at macromolecular crystallography beamlines. *J. Synchrotron Radiat.* **2002**, *9*, 401−406.

(31) Soltis, S. M.; Cohen, A. E.; Deacon, A.; Eriksson, T.; González, A.; McPhillips, S.; Chui, H.; Dunten, P.; Hollenbeck, M.; Mathews, I.; Miller, M.; Moorhead, P.; Phizackerley, R. P.; Smith, C.; Song, J.; van dem Bedem, H.; Ellis, P.; Kuhn, P.; McPhillips, T.; Sauter, N.; Sharp, K.; Tsyba, I.; Wolf, G. New paradigm for macromolecular crystallography experiments at SSRL: automated crystal screening and remote data collection. *Acta Crystallogr., Sect. D* **2008**, *64*, 1210−1221.

https://doi.org/10.1021/jacs.2c03376
J. Am. Chem. Soc. 2022, 144, 12769−12780

(32) McCoy, A. J.; Grosse-Kunstleve, R. W.; Adams, P. D.; Winn, M. D.; Storoni, L. C.; Read, R. J. Phaser crystallographic software. *J. Appl. Crystallogr.* **2007**, *40*, 658−674.
(33) Emsley, P.; Lohkamp, B.; Scott, W. G.; Cowtan, K. Features and development of Coot. *Acta Crystallogr., Sect. D: Biol. Crystallogr.* **2010**, *66*, 486−501.
(34) Adams, P. D.; Afonine, P. V.; Bunkoczi, G.; Chen, V. B.; Davis, I. W.; Echols, N.; Headd, J. J.; Hung, L. W.; Kapral, G. J.; Grosse-Kunstleve, R. W.; McCoy, A. J.; Moriarty, N. W.; Oeffner, R.; Read, R. J.; Richardson, D. C.; Richardson, J. S.; Terwilliger, T. C.; Zwart, P. H. PHENIX: a comprehensive Python-based system for macromolecular structure solution. *Acta Crystallogr., Sect. D: Biol. Crystallogr.* **2010**, *66*, 213−221.
(35) Afonine, P. V.; Grosse-Kunstleve, R. W.; Echols, N.; Headd, J. J.; Moriarty, N. W.; Mustyakimov, M.; Terwilliger, T. C.; Urzhumtsev, A.; Zwart, P. H.; Adams, P. D. Towards automated crystallographic structure refinement with phenix.refine. *Acta Crystallogr., Sect. D: Biol. Crystallogr.* **2012**, *68*, 352−367.
(36) Moriarty, N. W.; Grosse-Kunstleve, R. W.; Adams, P. D. electronic Ligand Builder and Optimization Workbench (eLBOW): a tool for ligand coordinate and restraint generation. *Acta Crystallogr., Sect. D: Biol. Crystallogr.* **2009**, *65*, 1074−1080.
(37) Moriarty, N. W.; Draizen, E. J.; Adams, P. D. An editor for the generation and customization of geometry restraints. *Acta Crystallogr., Sect. D: Struct. Biol.* **2017**, *73*, 123−130.
(38) Richter, G.; Krieger, C.; Volk, R.; Kis, K.; Ritz, H.; Götze, E.; Bacher, A. Biosynthesis of riboflavin: 3,4-dihydroxy-2-butanone-4-phosphate synthase[34] Biosynthesis of riboflavin: 3,4-dihydroxy-2-butanone-4-phosphate synthase. *Methods Enzymol.* **1997**, *280*, 374−382.
(39) Westerfeld, W. W. A Colorimetric Determination of Blood Acetion. *J. Biol. Chem.* **1945**, *161*, 495−502.
(40) Speckman, R. A.; Collins, E. B. Specificity of the Westfield adaptation of the Voges - Proskauer test. *Appl. Environ. Microbiol.* **1982**, *44*, 40−43.
(41) Antharavally, B. S.; Poyner, R. R.; Ludden, P. W. EPR Spectral Evidence for Binuclear Mn(II) Center in Dinitrogenase Reductase-Activating Glycohydrolase from *Rhodospirillum rubrum*. *J. Am. Chem. Soc.* **1998**, *120*, 8897−8898.
(42) Liebschner, D.; Afonine, P. V.; Moriarty, N. W.; Poon, B. K.; Sobolev, O. V.; Terwilliger, T. C.; Adams, P. D. Polder maps: improving OMIT maps by excluding bulk solvent. *Acta Crystallogr., Sect. D: Struct. Biol.* **2017**, *73*, 148−157.
(43) Plaut, G. W. E. Biosynthesis of riboflavin. II. Incorporation of C14-labeled compounds into ring A. *J. Biol. Chem.* **1954**, *211*, 111−116.
(44) Plaut, G. W. E.; Broberg, P. L. Biosynthesis of riboflavin. III. Incorporation of C14-labeled compounds into the ribityl side chain. *J. Biol. Chem.* **1956**, *219*, 131−138.
(45) Bryn, K.; Stormer, F. Decreased riboflavin formation in mutants of *Aerobacter (Enterobacter) aerogenes* deficient in the butanediol pathway. *Biochim. Biophys. Acta* **1976**, *428*, 257−259.
(46) Nakajima, K.; Mitsuda, H. Possibility of diacetyl and related compounds as the 4-carbon compound necessary for the formation of riboflavin in *Ashbya gossypii*. *Acta Vitaminol. Enzymol.* **1984**, *6*, 271−282.
(47) Jabasini, M. T.; Al-Khalidi, U. A. S. Asymmetric labelling of the xylene ring in riboflavin. *Int. J. Biochem.* **1975**, *6*, 735−739.
(48) Bresler, S. E.; Perumov, D. A.; Chernik, T. P.; Skvortsova, A. P. [Operon for riboflavin synthesis in *Bacillus subtilis*. XI. Determination of the type of regulation using a test for dominance of operator-constitutive and regulator-constitutive mutations]. *Genetika* **1976**, *12*, 124−130.
(49) Hollander, I. J.; Braman, J. C.; Brown, G. M. Biosynthesis of riboflavin: enzymatic conversion of 5-amino-2,4-dioxy-6-ribitylamino-pyrimidine to 6,7-dimethyl-8-ribityllumazine. *Biochem. Biophys. Res. Commun.* **1980**, *94*, 515−521.
(50) Alworth, W. L.; Dove, M. F.; Baker, H. N. Biosynthesis of the dimethylbenzene moiety of riboflavin and dimethylbenzimidazole: evidence for the involvement of C-1 of a pentose as a precursor. *Biochemistry* **1977**, *16*, 526−531.
(51) Hörig, J.; Renz, P. Biosynthesis of vitamin B12. Formation of free 5,6-dimethylbenzimidazole and alpha-ribazole from riboflavin by *Propionibacterium freudenreichii*. *FEBS Lett.* **1977**, *80*, 337−339.
(52) Hörig, J. A.; Renz, P.; Heckmann, G. [5-15N]Riboflavin as precursor in the biosynthesis of the 5,6-dimethylbenzimidazole moiety of vitamin B12. A study by ^{1}H and ^{15}N magnetic resonance spectroscopy. *J. Biol. Chem.* **1978**, *253*, 7410−7414.
(53) Kühnle, H. F.; Renz, P. Biosynthesis of 5,6-dimethylbenzimidazole. Precursor-function of 6,7-dimethyl-8-ribityllumazine. *Z. Naturforsch., B* **1971**, *26*, 1017−1020.
(54) Renz, P. Riboflavin as precursor in the biosynthesis of the 5,6-Dimethylbenzimidazole-moiety of vitamin B(12). *FEBS Lett.* **1970**, *6*, 187−189.
(55) Renz, P.; Weyhenmeyer, R. Biosynthesis of 5, 6-dimethylbenzimidazole from riboflavin Transformation of C-1′ of riboflavin into C-2 of 5, 6-dimethylbenzimidazole. *FEBS Lett.* **1972**, *22*, 124−126.
(56) Bacher, A.; Levan, Q.; Buehler, M.; Keller, P. J.; Eimicke, V.; Floss, H. G. Biosynthesis of Riboflavin—Incorporation of D-[1-C-13]-Labeled Ribose. *J. Am. Chem. Soc.* **1982**, *104*, 3754−3755.
(57) Floss, H. G.; Quang Le Van, Q.; Keller, P. J.; Bacher, A. Biosynthesis of Riboflavin - an Unusual Rearrangement in the Formation of 6,7-Dimethyl-8-Ribityllumazine. *J. Am. Chem. Soc.* **1983**, *105*, 2493−2494.
(58) Neuberger, G.; Bacher, A. Biosynthesis of riboflavin. An aliphatic intermediate in the formation of 6,7-dimethyl-8-ribityllumazine from pentose phosphate. *Biochem. Biophys. Res. Commun.* **1985**, *127*, 175−181.
(59) Fischer, M.; Römisch, W.; Schiffmann, S.; Kelly, M.; Oschkinat, H.; Steinbacher, S.; Huber, R.; Eisenreich, W.; Richter, G.; Bacher, A. Biosynthesis of riboflavin in archaea studies on the mechanism of 3,4-dihydroxy-2-butanone-4-phosphate synthase of *Methanococcus jannaschii*. *J. Biol. Chem.* **2002**, *277*, 41410−41416.
(60) Richter, G.; Kelly, M.; Krieger, C.; Yu, Y.; Bermel, W.; Karlsson, G.; Bacher, A.; Oschkinat, H. NMR studies on the 46-kDa dimeric protein, 3,4-dihydroxy-2-butanone 4-phosphate synthase, using 2H, 13C, and 15N-labelling. *Eur. J. Biochem.* **1999**, *261*, 57−65.
(61) Bürgi, H. B.; Dunitz, J. D.; Lehn, J. M.; Wipff, G. Stereochemistry of reaction paths at carbonyl centres. *Tetrahedron* **1974**, *30*, 1563−1572.
(62) Nakamura, K.; Osamura, Y. Theoretical-Study of the Reaction-Mechanism and Migratory Aptitude of the Pinacol Rearrangement. *J. Am. Chem. Soc.* **1993**, *115*, 9112−9120.

https://doi.org/10.1021/jacs.2c03376
J. Am. Chem. Soc. 2022, 144, 12769−12780